Thermal atomic layer deposition of rhenium nitride and rhenium metal thin films using methyltrioxorhenium

Journal:	*Dalton Transactions*
Manuscript ID	DT-ART-10-2021-003454.R2
Article Type:	Paper
Date Submitted by the Author:	19-Nov-2021
Complete List of Authors:	Cwik, Stefan; Wayne State University, Department of Chemistry Woods, Keenan; Applied Materials Inc Perera, S.; Wayne State University, Department of Chemistry Saly, Mark; Applied Materials, Process Chemistry Knisley, Thomas; Applied Materials Inc Winter, Charles; Wayne State University, Department of Chemistry

SCHOLARONE™
Manuscripts

Thermal atomic layer deposition of rhenium nitride and rhenium metal thin films using methyltrioxorhenium

Stefan Cwik,[a] Keenan N. Woods,[b] S. Sameera Perera,[a] Mark J. Saly,[b] Thomas J. Knisley,[b] and Charles H. Winter*,[a]

The growth of rhenium nitride and rhenium metal thin films is presented using atomic layer deposition (ALD) with the precursors methyltrioxorhenium and 1,1-dimethylhydrazine. Saturative, self-limiting growth was determined at 340 °C for pulse times of ≥4.0 s for methyltrioxorhenium and ≥0.1 s for 1,1-dimethylhydrazine. An ALD window was observed from 340 to 350 °C with a growth rate of about 0.60 Å/cycle. Films grown at 340 °C revealed an root mean square surface roughness of 2.7 nm for a 70 nm thick film and possessed a composition of $ReN_{0.14}$ with low O and C content of 1.6 and 2.6 at.%, respectively. Enhanced nucleation on *in-situ* grown TiN, relative to thermal SiO_2, enabled a conformality of 98% on high aspect ratio trenched structures. Subjecting the $ReN_{0.14}$ thin films to thermal or chemical and thermal treatments reduced the nitrogen content to ≤1.6 at.%, yielding a film purity of about 96 at.% rhenium and resistivities as low as 51 μΩ cm. The Re metal film thicknesses on the trenched structures remained intact during the post-deposition annealing treatments and the films did not delaminate from the substrate surfaces.

Introduction

Rhenium (Re) metal possesses many beneficial properties, including very high melting point (3180 °C), high strength at elevated temperatures, high hardness, excellent wear resistance, high surface binding energy, a work function of 4.72 eV, and low electrical resistivity (18.7 μΩ cm).[1-30] Potential applications include hard coatings, wear resistant coatings, catalysis, and various uses in microelectronics devices. Thin films of Re are required for many applications. Re and Re-containing thin films have been deposited by many methods, including various types of sputtering,[1-7] molecular beam epitaxy,[8,9] electroplating and electroless deposition,[10-16] and chemical vapor deposition (CVD).[17-30] CVD growth of Re metal and Re-containing films have mostly employed $ReCl_5$, but ReF_6, $Re_2(CO)_{10}$, $CpRe(CO)_3$, $HRe(CO)_5$, $MeReO_3$, and $EtReO_3$ have also been used as precursors.[17-30]

The ongoing miniaturization of semiconductor devices has led to an increasing focus on the evaluation of new materials with dimensions on the nanometer scale. There is particular interest in metals with low resistivities at thicknesses of <20 nm and good surface adhesion to substrates.[31,32] The high surface binding energy of Re metal[33] and its low bulk resistivity of 18.7 μΩ cm[34] make it a promising candidate for use in microelectronics devices. Applications of Re metal films in

microelectronics devices have been limited to date, but have included diffusion barriers for copper interconnects,[3,12,27] gate metals for transistors,[22,23] microwave resonators,[8] and materials in superconducting devices.[2,6]

Atomic layer deposition (ALD) is a film growth method that affords Angstrom level film thickness control and can give perfect conformal coverage in high aspect ratio features.[35,36] These attributes make ALD of special interest for microelectronics device manufacturing. The thermal ALD of ReN_x and Re metal films was recently reported using $ReCl_5$ and ammonia.[37] ReN_x films were obtained at temperatures below 400 °C, while temperatures of 400 °C or higher led to Re metal films through loss of N_2. The corrosive nature of $ReCl_5$ potentially limits its utility as a precursor, since underlying materials can be etched by the HCl byproduct. As such, there is a need for halogen-free precursors for Re metal ALD. In this regard, carbonyl-containing precursors such as $Re_2(CO)_{10}$, $ReCp(CO)_3$, and $HRe(CO)_5$ are potential ALD precursors, however, their use in CVD resulted in considerable carbon (C) incorporation in the resultant films.[19,28] Trioxorhenium compounds of the general formula $RReO_3$ have been evaluated as CVD precursors, and revealed promising precursor characteristics, especially for small alkyl groups (R = Me, Et).[25] Methyltrioxorhenium ($MeReO_3$, hereafter MTO) was found to be the most promising CVD precursor candidate because of its high volatility, good thermal stability, and low C impurities observed in ReO_x and Re films grown by plasma CVD.[25] More recently, MTO was used as an ALD precursor in combination with trimethylaluminum for the growth of the mixed metal oxide thin films $Re_xAl_yO_{3x}$[38] and $Re-Al_2O_3Me$.[39]

a. Department of Chemistry, Wayne State University, Detroit, Michigan 48202, USA.
   E-mail: chw@chem.wayne.edu.
b. Applied Materials, 974 East Arques Avenue, Sunnyvale, California 94085, USA.
†Electronic Supplementary Information (ESI) available: Film characterization data.
See DOI: 10.1039/x0xx00000x

In order to develop new ALD processes employing halogen-free Re precursors, the choice of the reducing co-reactant is of great importance, particularly because of the Re-O and Re-C bonds present in MTO. The ReCl₅-based ALD process employed ammonia as the co-reactant.[37] Complete reaction of MTO with the nitrogen (N) co-reactant is vital to avoid the formation of Re oxide nitride phases, since the stronger Re-O bonds could afford ReOₓ films upon annealing.

Herein, we report the thermal ALD of ReNₓ and Re metal films using MTO and 1,1-dimethylhydrazine (Me_2NNH_2). The basicity of alkyl hydrazines should be sufficient to react completely with MTO to form ReNₓ or Re with low C and O levels. ReNₓ films were deposited within an ALD window of 340 to 350 °C, but were transformed to high purity Re metal films upon annealing at ≥400 °C under various conditions. The films obtained in this study were fully characterized with respect to thickness, resistivity, structure, morphology, and composition using scanning electron microscopy (SEM), X-ray fluorescence (XRF), 4-point probe resistivity measurements, grazing incidence X-ray diffraction (GI-XRD), atomic force microscopy (AFM), and X-ray photoelectron spectroscopy (XPS). Additionally, films were deposited in trenched substrates, either on thermal SiO₂ or TiN surfaces. Transmission electron microscopy (TEM) was employed to assess the conformality of the depositions before and after annealing and also to understand the film continuity at low thicknesses.

Experimental

ALD experiments were performed with a Picosun R-75 BE ALD reactor at process temperatures ranging from 300 to 400 °C on SiO₂ (300 nm)/Si and TiN (20 nm)/Si substrates without removal of the native oxides. MTO (98% purity) was used as received from Strem Chemicals, Inc. and was delivered from a Picosolid booster into the reactor chamber at 35 °C at the reactor pressure of about 5-7 Torr. Linear relationships were observed in plots of MTO consumption versus number of growth cycles, which ruled out false self-limiting behavior through MTO vapor depletion in the booster. Me_2NNH_2 was purchased from Sigma-Aldrich and was delivered at room temperature, using a conventional vapor-draw bubbler. In order to limit the consumption of Me_2NNH_2, a flow restricting VCR gasket (100 μm) was installed in the bubbler line. Ultrahigh purity N₂ (99.999%, Airgas) was used as the carrier gas. Re thin films were deposited between 300 and 400 °C according the sequence 4.0 s MeReO₃ – 20 s purge – 0.1 s Me_2NNH_2 – 20 s purge, unless stated overwise. *In-situ* TiN was deposited according to a literature ALD process[40] with the pulse and purge sequence of 5 s TiCl₄ – 20 s purge – 0.5 s hydrazine – 20 s purge. Annealing under reactive atmosphere was performed in a CN1 (CN1 Co., Ltd.) reactor at 400 °C at 11-12 Torr for 1 h, followed by an annealing step in a tube furnace at 600 °C for 10 minutes in a N₂ atmosphere. The inert annealing was also solely performed in a tube furnace at 600 °C for 10 minutes in a N₂ atmosphere.

Cross-sectional film thickness measurements were performed with a JEOL-6510LV scanning electron microscope. The room temperature sheet resistivities were measured using a Jandel 4-point probe RM3000+. XRF measurements were carried out prior to and after the depositions using a Hitachi FT150h instrument. The Re Kα intensities were determined after 30 s measurements at a voltage of 45 kV with an Al500 primary filter and without a collimator. For TEM imaging, samples were prepared using an FEI Helios 600i scanning electron microscope and were subsequently imaged using an FEI ThemisTEM instrument (200 kV). XPS data were collected with a Thermo Fisher Scientific K-Alpha XPS system equipped with a monochromatic Al source (spot size 400 × 600 μm², 500 eV Ar ion sputtering, and 1.8×10^{-8} Torr working pressure). AFM images were collected using a DI7000 AFM (Digital Instruments, Inc.) in the noncontact mode (1 Hz scan rate).

Results and discussion

Precursor Selection and Initial Studies

The synthesis and properties of MTO have been previously reported.[41] The chemical structure of MTO is shown in Chart S1. MTO is a solid with a melting point of 111 °C and sublimation temperature of 65 °C at 0.001 Torr. The thermogravimetric analysis of MTO was previously reported, and shows a single step weight loss with no residual mass.[38] To address thermal stability under film growth conditions, MTO was pulsed into the reactor chamber without a co-reactant (500 cycles: 4.0 s MTO – 40 s purge) at substrate temperatures between 300 and 400 °C. Thermal decomposition was observed by XRF on metal substrates such as Co, Cu, Ru, and Pt (Fig. S1), which is consistent with a previous report that described film growth in CVD using MTO on steel surfaces at temperatures above 300 °C.[25] By contrast, no film growth was observed on Si, SiO₂, TiN, and TaN at temperatures of up to 400 °C by XRF (Fig. S1). Moreover, the sheet resistances of the latter substrates remained unchanged after the attempted depositions. The etching behavior of MTO with metal substrates was also explored. Pulsing as described above with only MTO using Ru, Co, and Cu substrates at 340 °C afforded no detectable decreases in the metal XRF signals after 1000 cycles (Fig. S2), demonstrating a lack of metal etching by MTO. ReCl₅ was previously used as a precursor for Re metal ALD,[37] and is a potential etchant for metal films. Pulsing only ReCl₅ over Ru, Co, and Cu substrates at 400 °C (the temperature required for the growth of Re metal films[37]) using the pulse sequence 4.0 s ReCl₅ – 40 s purge with 500 cycles led to significant decreases in the intensities of the Co and Cu XRF signals, indicating etching by ReCl₅ (Fig. S3). The XRF signal intensities for Ru substrates were similar before and after ReCl₅ treatment (Fig. S3), suggesting no etching. The lack of metal

substrate etching by MTO is a significant advantage compared to the etching induced by $ReCl_5$.

Self-limiting growth

To assess self-limiting growth, the saturation behavior of the MTO precursor and Me_2NNH_2 co-reactant was studied at 340 °C for 500 deposition cycles. For MTO, the pulse time of Me_2NNH_2 was set at 0.1 s and 20 s N_2 purges were used to ensure removal of volatile species. A plot of growth rate versus MTO pulse times demonstrated a saturative growth rate of 0.60 Å/cycle at ≥3.0 s pulse lengths (Fig. 1a). Film thicknesses were determined by cross-sectional SEM. However, the film resistivity reached a minimum value at ≥4.0 s MTO pulse lengths. Therefore, a 4.0 s MTO pulse length was employed for the experiments described below. A plot of growth rate versus Me_2NNH_2 pulse length revealed a constant growth rate of 0.60 Å/cycle at 0.1 to 0.3 s pulse lengths (Fig. 1b). However, the film resistivity was lowest at 0.1 s pulse length, so this value was chosen. Based upon these experiments, a pulse and purge recipe of 4.0 s MTO pulse – 20 s N_2 purge – 0.1 s Me_2NNH_2 pulse – 20 s N_2 purge was employed for all subsequent deposition experiments. The saturative MTO pulse lengths were additionally determined by XRF, revealing increasing Re content up to 4.0 s pulse time (Fig. S4). These XRF experiments mirror the thickness data shown in Fig. 1 and support the interpretation of the resistivity data. The Re Lα XRF counts remained constant during the variation of the Me_2NNH_2 pulse lengths within experimental error (Fig. S5).

(b)

(a)
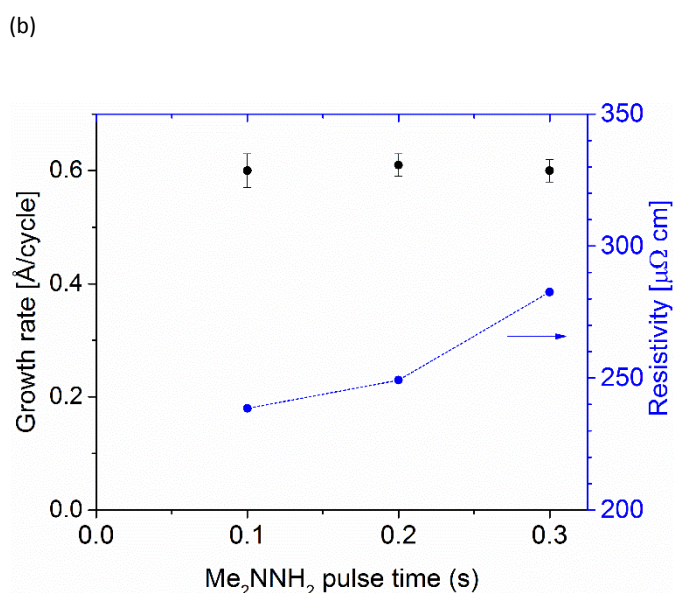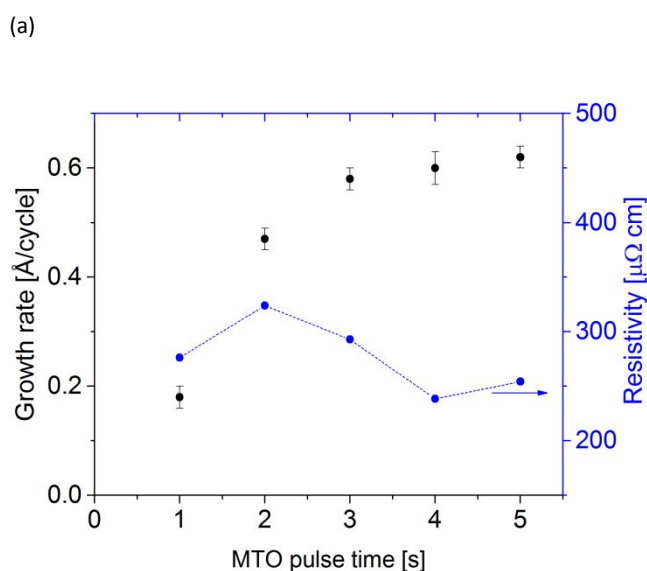
Fig. 1 Dependence of growth rate on precursor pulse length for MTO (a) and Me_2NNH_2 (b) at 340 °C using 500 cycles on SiO_2 with thicknesses evaluated by cross-sectional SEM.
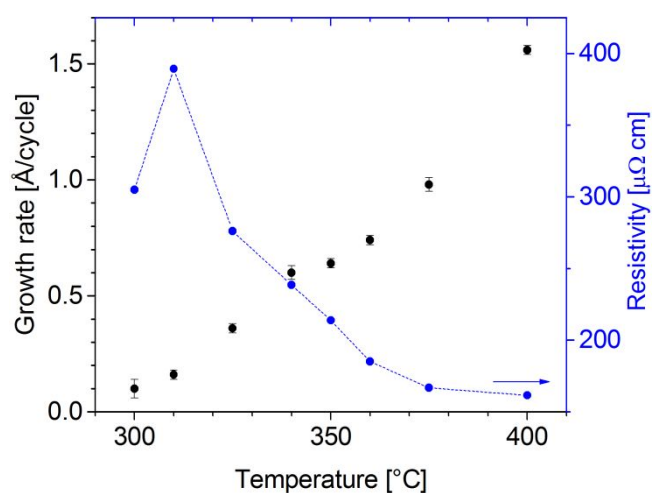
Temperature series

At optimized pulse times for MTO and Me_2NNH_2, a series of depositions was carried out in the range from 300 to 400 °C to evaluate a potential ALD window and to gain insight into the film resistivities with respect to deposition temperature (Fig. 2). The growth rate increased steadily with temperature up to an ALD window between 340 to 350 °C. The growth rate in the ALD window was about 0.60 Å/cycle, consistent with the saturation curves in Fig. 1. At temperatures above 350 °C, the growth rate increased up to 1.5 Å/cycle at 400 °C, most likely due to thermal decomposition of MTO. MTO was previously reported to decompose between 300 and 350 °C.[25] While no growth was observed on SiO_2 substrates using only MTO as the precursor, the experiments in Fig. 2 involved ALD growth with MTO and Me_2NNH_2. Accordingly, the presence of Me_2NNH_2 must change the surface chemistry to allow the chemisorption of MTO. The film resistivities were about 250 μΩ cm within the ALD window, but ranged from 275 to 400 μΩ cm at ≤330 °C. Uncertainties in resistivity values are about ±10%, largely because of film thickness

measurement uncertainties by SEM. At temperatures of ≥350 °C, the resistivity values decreased and reached a minimum of 160 μΩ cm at 400 °C. The decreasing resistivities with increasing deposition temperatures is probably related to decreasing N content in the films due to thermal decomposition of ReN_x at elevated temperatures. ReN_x is reported to be metastable and releases nitrogen at elevated temperatures (≥400 °C).[4,37] The growth rates changes observed upon increasing the deposition temperatures were confirmed by XRF results for the samples grown on SiO_2 substrates (Fig. S6).
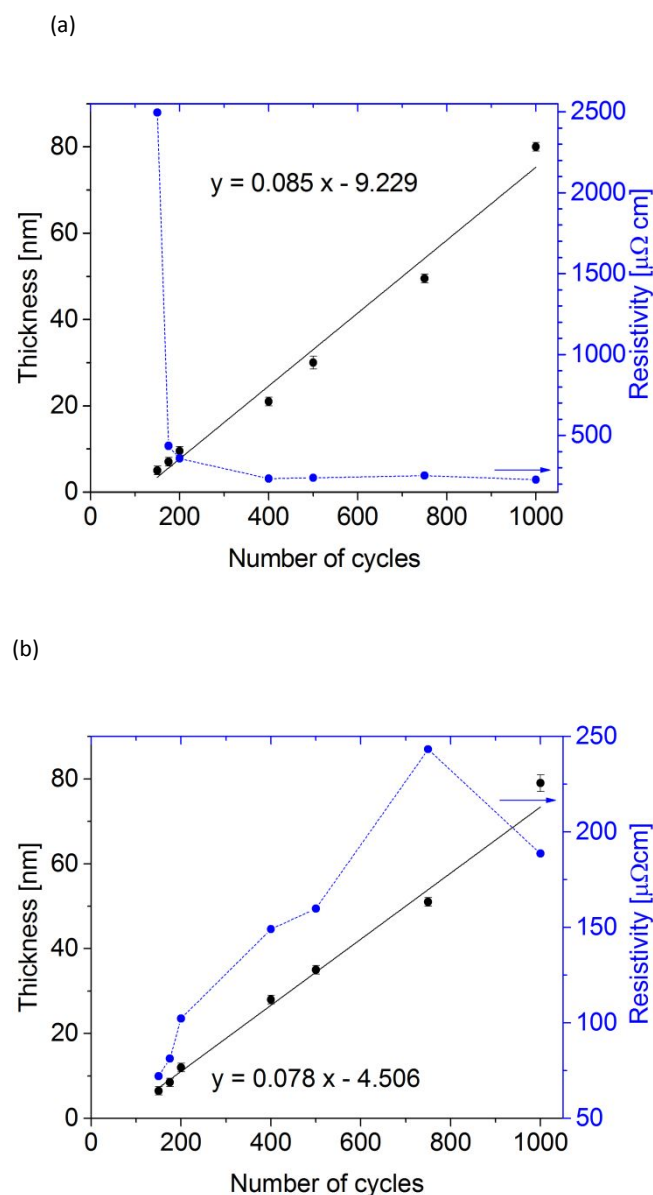
at thicknesses of >10 nm to about 230 μΩ cm. Films deposited on TiN had resistivities below 100 μΩ cm for thicknesses of <10 nm, which originates from the conductivity of the underlying TiN substrates. Resistivites for 58 and 78 nm thick films grown on TiN were 185 and 245 μΩ cm, which are similar to the values observed for thicker films on SiO_2.

Fig. 2 Dependence of growth rate on the deposition temperature for films grown from 300 to 400 °C with 500 cycles on SiO_2. Thicknesses were evaluated by cross-sectional SEM.

Dependence of film thicknesses on the number of growth cycles

The dependence of the film thickness on the number of growth cycles is shown in Fig. 3 for SiO_2 and TiN substrates. These films were grown at 340 °C using the optimized pulse sequences described above. The growth rates for these processes were 0.85 Å/cycle on SiO_2 and 0.78 Å/cycle on TiN (Fig. 3), using cross-sectional SEM to measure film thicknesses (Figs. S7-S10). These values are higher than the growth rate of ~0.60 Å /cycle observed in Figs. 1 and 2, since they do not include nucleation delays of ~109 cycles on SiO_2 and ~58 cycles on TiN. It is possible that the lower growth rate on TiN substrates arises from more efficient nucleation and the formation of denser films, compared to SiO_2. Plots of XRF $ReL\alpha$ signals as a function of number of growth cycles also provided linear relationships, with growth rates of 0.96 and 0.98 Å/cycle on SiO_2 and TiN substrates, respectively (Fig. S11). These growth rates suggest that similar amounts of Re are deposited on SiO_2 and TiN substrates, supporting the proposal of denser films on TiN substrates. Nucleation delays from the XRF plots were ~113 cycles on SiO_2 and ~64 cycles on TiN, which are identical to the values obtained from the plots using SEM thickness measurements. Resistivities of <10 nm thick films grown on SiO_2 were ~2500 μΩ cm, but decreased sharply

(a)

(b)

Fig. 3 Dependence of film thickness on the number of growth cycles for films grown at 340 °C on SiO_2 (a) and TiN (b), as evaluated by SEM. The r^2 values are 0.98484 (a) and 0.99119 (b).

Film compositions

The composition of a 70 nm thick Re film grown on a Si(100) substrate with native oxide at 340 °C for 1000 cycles was investigated by XPS with sequential Ar ion sputtering. The depth profile (Fig. 4) revealed surface oxides that were removed upon Ar ion sputtering. After 600 s of sputtering, a constant composition was obtained and is summarized in Table 1. A Re content of 83.8 at.% was observed and both C (2.6 at.%) and O (1.6 at.%) were present at low levels. The remainder of the film composition was 12 at.% of N, which indicates formation of nitride species during film growth. Ignoring the C and O, the overall composition of the film is $ReN_{0.14}$. The low O content suggests a complete reaction of the oxide ligands in MTO to Re metal and ReN_x. The low C content implies efficient removal of the methyl group in MTO and minimal C incorporation from the methyl groups in Me_2NNH_2.

energy of 40.7 eV corresponds to Re metal, which has been reported to range from 40.3 to 40.8 eV.[42-45] The additional presence of Re-N bonds is indicated by the ionization at 42.3 eV, since the ReN_x ionization appears at around 42.2 eV.[46] The N 1s binding energy of 397.7 eV corresponds to a metal nitride.[44] The minor ionization at 399.8 eV may correspond to an organic N species.[44] The O 1s ionization (Fig. S12) shows a typical oxide binding energy of 530.6 eV.[44] The C 1s ionization at 283.8 eV (Fig. S12) might be attributable to aliphatic C embedded into the film during Re growth.[44] This is agreement with a literature report ruling out rhenium carbide formation.[29] The intensities of the O 1s and C1s ionizations were very low, which precluded peak modelling to obtain more detailed information.

(a)

Fig. 4 XPS depth profile of a 70 nm thick Re film grown at 340 °C on a Si(100) with native oxide substrate.

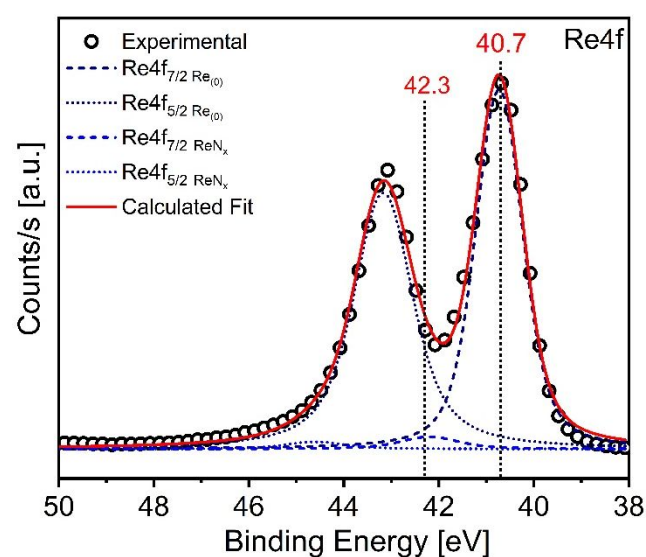**Table 1** Re thin film bulk composition as evaluated by XPS.

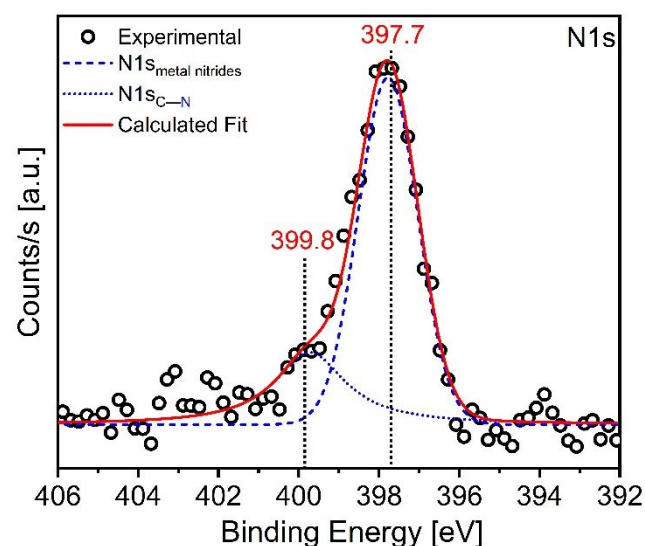|	Re $4f_{7/2}$	N 1s	O 1s	C 1s
Concentration [at. %]	83.8	12.0	1.6	2.6

The high resolution XPS spectra of the Re and N ionization regions in the film bulk are presented in Fig. 5. The Re $4f_{7/2}$ binding

(b)

**ARTICLE**

Fig. 5 High resolution Re 4f (a) and N 1s (b) ionization regions in the film bulk of a 70 nm Re film grown at 340 °C on a Si(100) with native oxide substrate.

Structure and morphology

For the study of the surface morphology, a 70 nm thick film grown on Si(100) with native oxide substrate at 340 °C was investigated by AFM (Fig. 6) and the root mean square (RMS) roughness was evaluated. An RMS surface roughness of 2.7 nm was observed, which is about 4% of the film thickness. The film surface is thus very smooth.
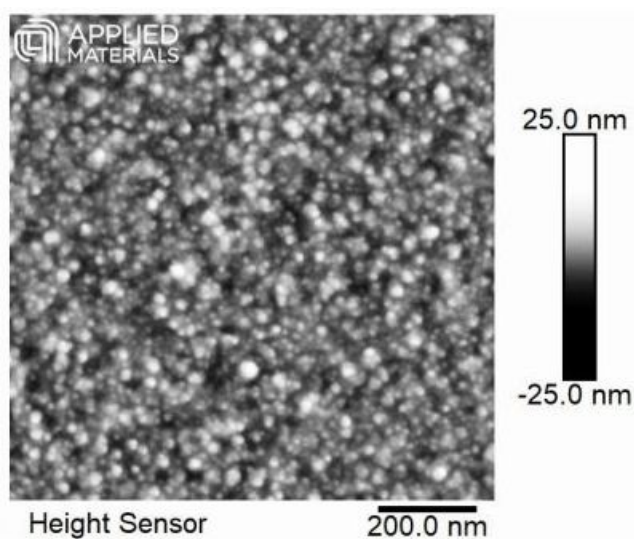
Fig. 6 AFM micrograph of a 70 nm thick film grown at 340 °C on a Si(100) with native oxide substrate.

X-ray diffraction experiments showed that films grown within the ALD window (340 to 350 °C) were amorphous. However, crystalline Re metal films were grown using MTO and Me_2NNH_2 with a substrate temperature of 400 °C, as revealed by GI-XRD (Fig. 7). The main reflection at $2\theta = 40°$ corresponds to Re metal in the (002) orientation. Fig. 7 also shows the positions of the (100) and (101) reflections for Re metal, which were not observed in our sample. The additional reflection at $2\theta = 45°$ is consistent with the coexistence of ReN_x, even at this elevated temperature.[37] The presence of ReN_x at a substrate temperature of 400 °C suggests that an additional post-deposition treatment is required to obtain pure Re metal, since the N evolution was incomplete.
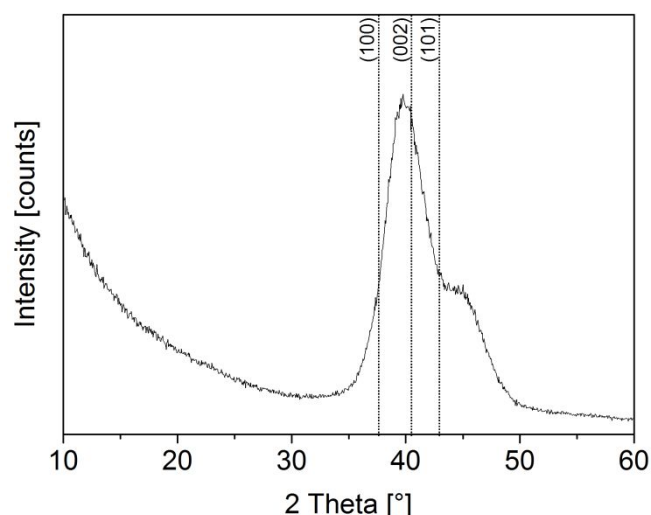

Fig. 7 GI-XRD pattern of a film grown at 400 °C for 500 cycles on a Si(100) with native oxide substrate.

Conformality Studies in High Aspect Ratio Features

The nucleation behavior was studied with respect to the substrate chemistry using trenched SiO_2 substrates containing aspect ratios of about 6.5, widths of about 15 nm, and depths of about 100 nm. ALD experiments were carried out at 340 °C on the untreated SiO_2 structures and on *in-situ* TiN covered structures that were coated with about 1 nm of *in situ*, ALD-grown TiN. The coated structures were studied by TEM. For the *in-situ* ALD TiN, $TiCl_4$ and hydrazine were used at 300 °C using the pulse and purge sequence 5 s $TiCl_4$ – 20 s N_2 purge – 0.5 s hydrazine – 20 s N_2 purge.[40,47] As shown in Fig. 8, nucleation of the film on the SiO_2 structures was modest and afforded non-homogeneous, non-continuous nanoparticles. By contrast, excellent nucleation behavior was observed on the *in-situ* TiN-coated structures, yielding a dense, continuous film. The conformal coverage was 98%. These findings are consistent with the differential nucleation delays on SiO_2 and TiN substrates described above. Moreover, Re diffusion into the underlying SiO_2 layer was observed on top regions of the trenched structures (Fig. 9). The *in-situ* 1 nm thick TiN liner revealed excellent barrier layer properties, since no diffusion was observed for this sample (Fig. 9).

(a)
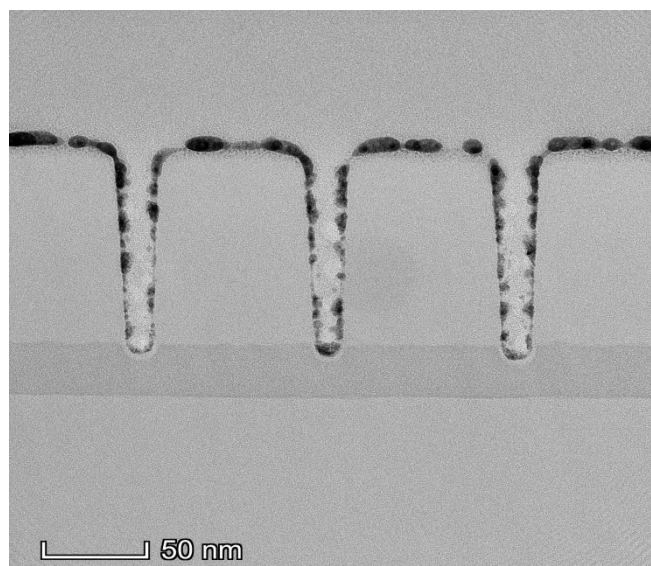
(b)
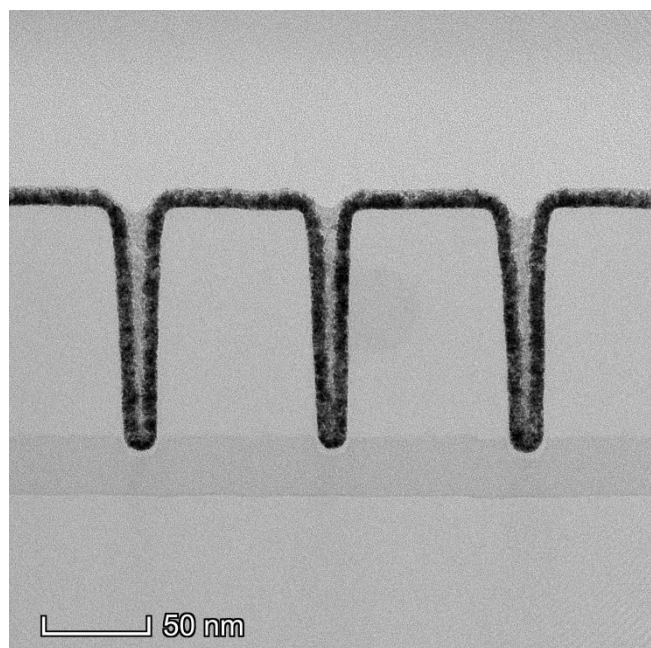
Fig. 8 TEM images of Re thin film grown on (a) SiO$_2$ trenched structures and (b) on *in-situ* 1 nm thick TiN coated structures.
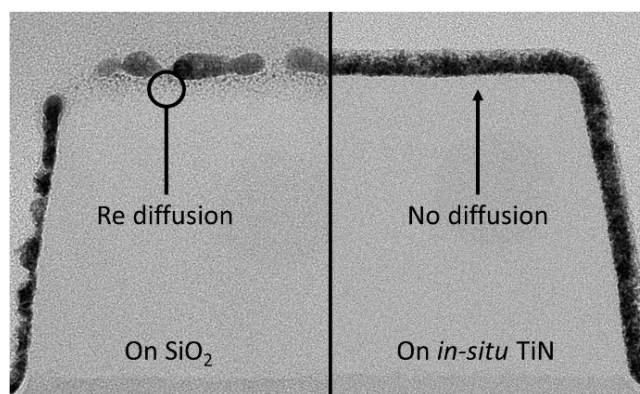
Fig. 9 Expansion of TEM images to highlight Re diffusion into SiO$_2$ (left), in contrast to no Re diffusion into TiN (right).
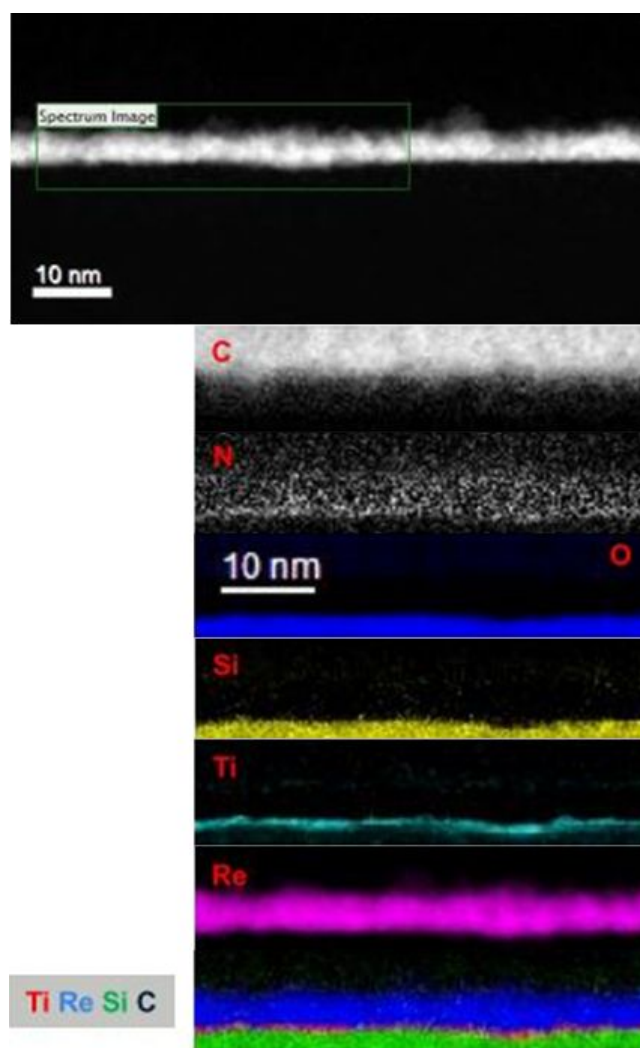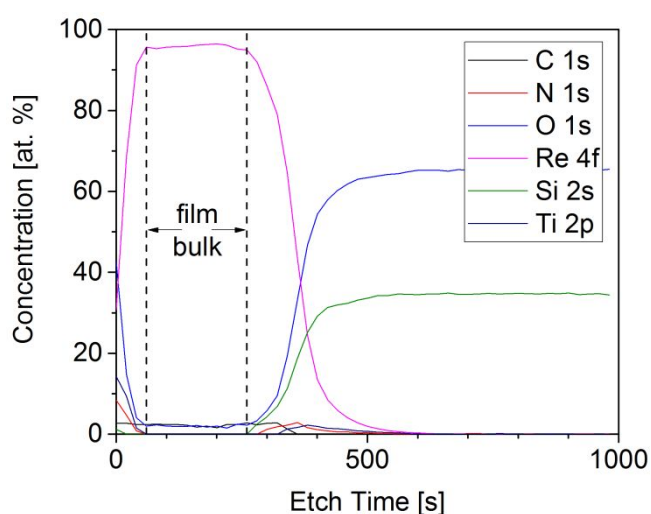

Fig. 10 TEM image and EELS elemental mapping for C, N, O, Si, Ti, and Re of a 3.6 nm Re film on 1 nm TiN on SiO$_2$, including an overlay of the elements C, Si, Ti, and Re.

The barrier layer properties of the *in-situ* TiN film were further analyzed by elemental mapping. In this experiment, a 1 nm thick *in-situ* TiN film was deposited on the SiO_2 structure, followed by the growth of a 3.6 nm $ReN_{0.14}$ film. After the confirmation of the film continuity of the Re thin film with TEM (Fig. 10), the elemental mapping was conducted with electron energy loss spectroscopy (EELS). No indication of metal diffusion was observed in the element maps (Fig. 10) or in the respective depth profile (Fig. S13). Additionally, the low oxygen level in the Re thin film was confirmed, which was below detection limit of EELS.

Annealing study of the $ReN_{0.14}$ films

The ultimate goal of this work was to develop ALD-based routes to Re metal films, not ReN_x films. Accordingly, the $ReN_{0.14}$ films that were deposited at 340 °C were annealed to study changes in composition, resistivity, and conformality. To assess the composition changes upon thermal treatment, a 20 nm thick film was analyzed by XPS prior to and after post deposition treatment. The as-deposited sample revealed a similar bulk composition (Table 2) as described in Table 1, highlighting the reproducibility of the process. To assess N_2 desorption, a 20 nm thick film was heated to 600 °C for 10 minutes under a high purity N_2 atmosphere. The XPS depth profile of the annealed film (Fig. 11) revealed an increased Re content in the film of 96 at.%. During the post-deposition treatment, N is completely removed from the film bulk and is only present at the film surface and in the TiN liner. Additionally, both C and O content decreased in the annealing step. We attribute the surface N content in the film prior to sputtering to N-containing organic residues, since they are easily removed upon sputtering. The resistivity of the thin film decreased from 140 μΩ cm prior to annealing to 74 μΩ cm after annealing. For comparison, the bulk resistivity of Re metal is 18.7 μΩ cm.

Table 2 Re thin film bulk composition as evaluated by XPS and resistivities before and after annealing.

	Re $4f_{7/2}$ [at.%]	N 1s [at.%]	O 1s [at.%]	C 1s [at.%]	Resistivity [μΩ cm]
As deposited	83.7	10.2	2.7	3.4	140
N_2 anneal	95.8	0.2	1.2	2.8	74
H_2 anneal	89.3	1.6	1.9	7.2	117
NH_3 anneal	95.8	0.4	2.1	1.8	51

The successful purification under inert annealing conditions motivated the subsequent study of reactive annealing, where the sample was treated at 400 °C under a reactive atmosphere (H_2 or NH_3) prior to annealing at 600 °C under argon. XPS data for these annealed films are shown in Figs. S14 and S15. While the H_2 pretreatment was found to be less efficient (resistivity after annealing 117 μΩ cm) than the pure thermal treatment (resistivity after annealing 74 μΩ cm), the annealing under an ammonia atmosphere improved the bulk resistivity further down to 51 μΩ cm. However, the compositions obtained by XPS are similar for all three annealed samples. Both Re and N contents are identical within experimental error for films annealed under H_2 and NH_3. The exception is the reduced C content for the ammonia annealed sample, which could be caused by the formation of volatile hydrocarbons due to ammonia exposure. Any Re nitrides that form upon treatment of Re metal with ammonia at 400 °C would eliminate N_2 from the films in the subsequent 600 °C annealing step. The resistivities of the annealed films (51-117 μΩ cm) did not approach the value for bulk Re metal (18.7 μΩ cm) after annealing. The slightly higher resistivity values after annealing may arise from the small amounts of C and O remaining in the films.

Fig. 11 XPS depth profile of an annealed Re thin film. The initial ReN_x film was about 20 nm thick.

Finally, the effects of annealing on a 20 nm Re thin film deposited on a trenched structure coated with 1 nm of in situ TiN were studied. The high surface binding energy of Re[33] was expected to allow thermal treatment without delamination from the trench walls. A continuous film was grown on the trenched structure, as confirmed by TEM (Fig. 12a). There was no noticeable roughening of the film surface by TEM after the annealing. Features grown in the trenches show a typical "keyhole" gap in the center of each trench, where precursors are unable to penetrate and fill. The coated trenched

structure was then annealed at 600 °C for 10 minutes and was then analyzed by TEM (Fig. 12b). The annealing step induced changes in the microstructure as evident from the presence of crystalline domains. Interestingly, the film thicknesses decreased only by <5%, suggesting that the density is close to the bulk value for Re metal of 21.02 g/cm³. Most importantly, excellent adhesion of Re was observed, since the films did not delaminate to a significant extent from the trenched structure walls. However, the small amount of shrinkage upon annealing led to some tiny gaps at the sides and bottoms of the structures between the SiO_2 substrate and the Re/TiN filling. Due to the high melting point of Re metal, it did not flow into the trenches. However, the annealing step reduced the keyhole sizes and fused the tops of the layers in each trench. Similar observations were obtained for the films that were subjected to the reactive annealing procedures (Figs. S16, S17), which highlights the tendency of thin Re metal films to adhere strongly to substrate surface and not undergo distortion upon annealing at 600 °C.
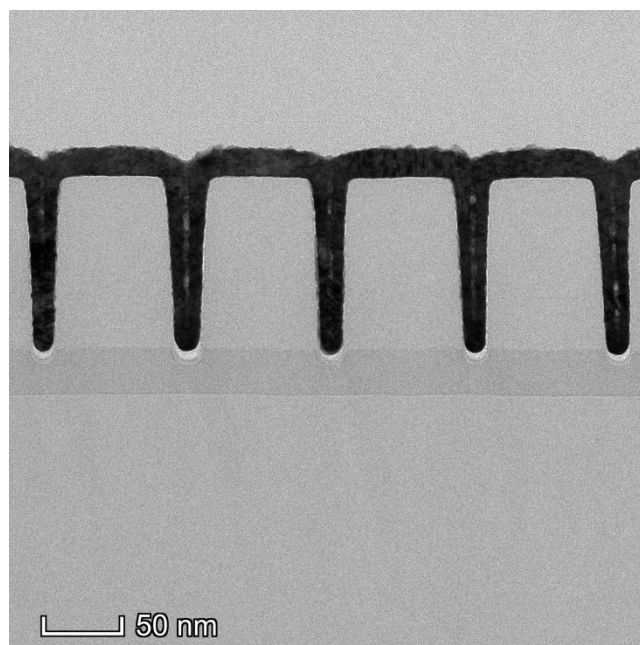
Fig. 12 TEM images of films grown on *in-situ* 1 nm TiN coated structures before (a) and after (b) annealing at 600 °C under inert atmosphere.

(a)
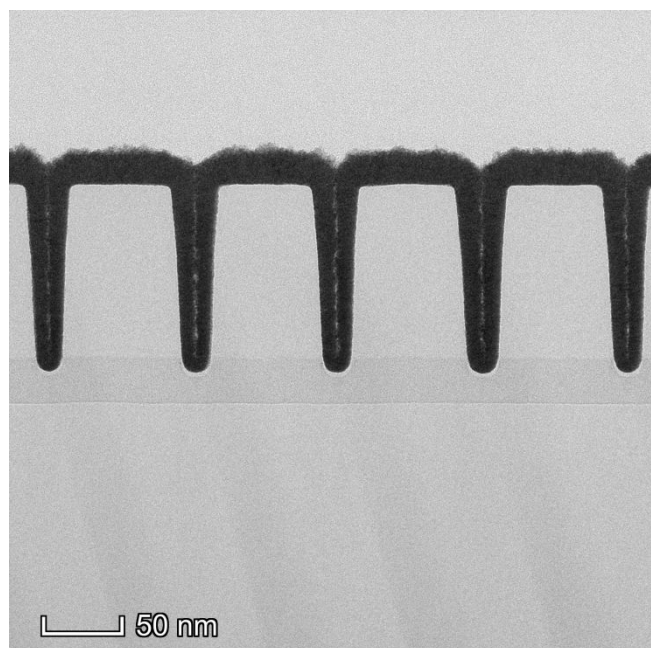
(b)

Mechanistic Possibilities

Key features in the deposition of ReN_x films from MTO and Me_2NNH_2 include low O and C levels in the films and N incorporation in the films. Imido complexes of the formula $RRe(NR')_3$ (R = Me,[48-50] $OSiMe_3$,[51] $OSiPh_3$;[52] R' = alkyl, aryl) have been reported, but were prepared by treatment of $RReO_3$ with either $RNHSiMe_3$ or RNCO. By contrast, treatment of MTO with primary amines $R'NH_2$ at room temperature affords the adducts $MeReO_3(NH_2R)$.[53,54] We speculate that treatment of MTO with Me_2NNH_2 under the high temperature ALD conditions described herein may lead to the hydrazido complex $MeRe(NNMe_2)_3$ as a film growth intermediate, thereby eliminating the O atoms from MTO as water. Protonation of the Re-C bond in MTO by Me_2NNH_2 would lead to elimination of the methyl group as methane. The low C content in the ReN_x and Re metal films suggests that cleavage of the relatively weak N-N bonds in $MeRe(NNMe_2)_3$ occurs to eliminate the dimethylamino groups as volatile species that are not incorporated in the films.

Conclusions

Herein, a thermal ALD process for the growth of Re nitride and Re metal films is presented. The process affords thin, conformal, and continuous films on high aspect ratio structures because of the self-limiting nature of ALD. Significantly, the metal-organic precursor MTO is halogen-free and does not etch sensitive metal substrates such as Co and Cu. By contrast, $ReCl_5$

causes extensive etching of Co and Cu substrates, as demonstrated herein. The co-reactant Me_2NNH_2 possesses sufficient reactivity to cleave the Re-O and Re-C bonds in MTO to afford films of the composition $ReN_{0.14}$ within the ALD window at 340 °C, with C and O contents below 3 at.%. Growth of films on trenched SiO_2 wafers generally showed poor nucleation and gave low conformal coverage and non-continuous coatings in the high aspect ratio features. However, growth of a 1 nm thick TiN layer on the SiO_2 surfaces of the trenched substrates allowed the deposition of conformal, dense, and continuous films. Additionally, the TiN layer served as a diffusion barrier to stop the infiltration of Re into the SiO_2 substrate surface. Thermal and reactive annealing procedures were investigated to convert the initial $ReN_{0.14}$ films into Re metal films through N_2 loss. These procedures afforded Re metal films with N contents of ≤1.6 at.% and resistivities as low as 51 μΩ cm. The thermal annealing of Re-coated trenched structures led to a small amount of densification, but delamination of the Re film from the TiN/SiO_2 surface was not observed, except for tiny gaps that occurred at the sidewalls and bottoms of the trenches. The high density and high surface binding energy of Re metal contribute to the thermal stability of the Re films.

Conflicts of interest

There are no conflicts of interest to declare.

Acknowledgements

References

1   M. Arroyave, G. Bejarano, J. David and J. Hernandez, *Thin Solid Films*, 2021, **733**, 138809.
2   G.-M. Xue, H.-F. Yu, Y. Tian, W.-Y. Liu, H.-W. Yu, Y.-F. Ren and S.-P. Zhao, *Chinese Phys. B*, 2013, **22**, 97401.
3   J. P. Chu, C. H. Lin, P. L. Sun and W. K. Leau, *J. Electrochem. Soc.*, 2009, **156**, H540-H543.
4   G. Soto, A. Rosas, M. H. Farias, W. De la Cruz and J. A. Diaz, *Mater. Character.*, 2007, **58**, 519-526.
5   S. Oh, D. A. Hite, K. Cicak, K. D. Osborn, R. W. Simmonds, R. McDermott, K. B. Cooper, M. Steffen, J. M. Martinis and D. P. Pappas, *Thin Solid Films*, 2006, **496**, 389-394.
6   K. L. Jiao, L. H. Chang, R. Wallace and W. A. Anderson, *Appl. Supercond.*, 1995, **3**, 55-60.
7   H. Danielson, B. Kasemo and L. Marklund, *Thin Solid Films*, 1971, **9**, 121-132.
8   E. Dumur, B. Delsoi, T. Weiβl, B. Kung, W. Guichard, C. Hoarau, C. Naud, K. Hasselback, O. Buisson, K. Ratter and B. Gilles, *IEEE Trans. Appl. Supercond.*, 2016, **26**, 1501304.
9   P. B. Welander, *J. Appl. Phys.*, 2010, **108**, 103508.
10 D. P. Pappas, D. E. David, R. E. Lake, M. Bal, R. B. Goldfarb, D. A. Hite, E. Kim, H.-S. Ku, J. L. Long, C. R. H. McRae, L. D. Pappas, A. Roshko, J. G. Wen, B. L. T. Plourde, I. Arslan and X. Wu, *Appl. Phys. Lett.*, 2018, **112**, 182601.
11 O. Berkh, L. Burstein, A. Gladkikh, N. Eliaz and E. Gileadi, *J. Electrochem. Soc.*, 2016, **163**, D295-D299.
12 S.-Y. Chang, L.-P. Liand, L.-C. Kao and C.-F. Lin, *J. Electrochem. Soc.*, 2015, **162**, D96-D101.
13 A. Duhin, A. Rozenblat-Raz, L. Burstein, A. Inberg, D. Horvitz, Y. Shacham-Diamand, N. Eliaz and E. Gileadi, *Appl. Surf. Sci.*, 2014, **313**, 159-165.
14 A. Duhin, A. Inberg, N. Eliaz and E. Gileadi, *Electrochim. Acta*, 2011, **56**, 9637-9643.
15 E. Muñoz, R. Schrebler, R. Henríquez, C. Heyser, P. A. Verdugo and R. Marotti, *Thin Solid Films*, 2009, **518**, 138-146.
16 W. D. Sides, E. Hassani, D. P. Pappas, Y. Hu, T.-S. Oh and Q. Huang, *J. Appl. Phys.*, 2020, **127**, 085301.
17 Y. Tong, S. Bai, H. Zhang and Y. Ye, *Appl. Surf. Sci.*, 2012, **261**, 390-395.
18 L. Zhu, S. Bai and K. Chen, *Surf. Coatings Technol.*, 2012, **206**, 4940-4946.
19 N. V. Gelfond, N. B. Morozova, E. S. Filatov, S. A. Gromilov and I. K. Igumenov, *J. Struct. Chem.*, 2009, **50**, 1126-1133.
20 H. C. King, M. C. Renier, K. E. Ellzey and W. J. Lackey, *Chem. Vap. Deposition*, 2003, **9**, 59-63.
21 W. Garrett, A. J. Sherman and J. Stiglich, *Mater. Manuf. Processes*, 2006, **21**, 618–620.
22 J. Pan, D. Canaperi, R. Jammy, M. Steen, J. Pellerin and M.-R. Lin, *IEEE Electron Dev. Lett.*, 2004, **25**, 775-777.
23 R. P. Pezzi, M. Copel, M. Gordon, E. Cartier and I. J. Baumvol, *Appl. Phys. Lett.*, 2006, **88**, 243509.
24 Y. Hirohata, M. Okegawa, H. Yanagihara, T. Hino, N. Ogiwara, J. Yagyu and M. Saidoh, *Vacuum*, 1999, **53**, 309–312.
25 W. A. Herrman, W. M. Wachter, F. E. Kühn and R. W. Fischer, *J. Organomet. Chem.*, 1998, **553**, 443-452.
26 D. Mittendorf and G. A. West, *Mater. Manuf. Processes*, 1998, **13**, 749–755.
27 E. Blanquet, A. M. Dutron, V. Ghetta, C. Bernard and R. Madar, *Microelectron. Eng.*, 1997, **37-38**, 189–195.
28 D. G. Anderson, N. Anwar, B. J. Aylett, L. G. Earwaker, M. I. Nasir, J. P. G. Farr, K. Stiebahl and J. M. Keen, *J. Organomet. Chem.*, 1992, **437**, C7-C12.
29 A. J. Sherman, R. H. Tuffias and R. B. Kaplan, *JOM*, 1991, **43**, 20–23.
30 K. T. Kim and G. Welsch, G. *Mater. Lett.*, 1991, **12**, 229–232.
31 D. Gall, *J. Appl. Phys.*, 2020, **127**, 050901.
32 D. Gall, *J. Appl. Phys.*, 2016, **119**, 085101.
33 K. J. Kanarik, S. Tan and R. A. Gottscho, *J. Phys. Chem. Lett.* 2018, **9**, 4814-4821.
34 Y. Isobe, M. Tanaka, S. Yamanaka and M. Miyake, *J. Less Common Metals*, 1989, **152**, 177-184.
35 M. Leskelä and M. Ritala, *Angew. Chem. Int. Ed.*, 2003, **42**, 5548–5554.
36 S. M. George, *Chem. Rev.*, 2010, **110**, 111–131.
37 J. Hämäläinen, K. Mizohata, K. Meinander, M. Mattinen, M. Vehkamäki, J. Räisänen, M. Ritala and M. Leskelä, *Angew. Chem. Int. Ed. Engl.*, 2018, **57**, 14538-14542.
38 M. Rimoldi, J. T. Hupp and O. K. Farha, *ACS Appl. Mater. Interfaces*, 2017, **9**, 35067–35074.
39 M. Gebhard, S. Letourneau, D. J. Mandia, D. Choudhury, A. Yanguas-Gil, A. Mane, A. P. Sattelberger and J. W. Elam, *Chem. Mater.*, 2019, **31**, 7821–7832.
40 S. Wolf, M. Breeden, I. Kwak, J. H. Park, M. Kavrik, M. Naik, D. Alvarez, J. Spiegelman and A. C. Kummel, *Appl. Surf. Sci.*, 2018, **462**, 1029–1035.
41 W. A. Herrmann, F. E. Kühn, R. W. Fischer, W. R. Thiel and C. C. Romao, *Inorg. Chem.*, 1992, **31**, 4431-4432.
42 M. D. Detwiler, P. Majumdar, X.-K. Gu, W. N. Delgass, F. H. Ribeiro, J. Greeley and D. Y. Zemlyanow, *Surf. Sci.*, 2016, **640**, 2-9.
43 A. Ramstad, F. Strisland, S. Raaen, T. Worren, A. Borg and C. Berg, *Surf. Sci.*, 1999, **524**, 57-67.

44 C. D. Wagner and G. E. Muilenberg, *Handbook of X-Ray Photoelectron Spectroscopy: A Reference Book of Standard Data for use in X-Ray Photoelectron Spectroscopy*, Physical Electronics Division, Perkin Elmer Corp., 1979.

45 A. S. Duke, R. P. Galhenage, S. A. Tenney, P. Sutter and D. A. Chen, *J. Phys. Chem. C*, 2014, **119**, 381-391.

46 S. Oktay, Z. Kahraman, M. Urgen and K. Kazmanli, *Appl. Surf. Sci.*, 2015, **328**, 255-261.

47 S. Cwik, K. N. Woods, M. J. Saly, T. J. Knisley and C. H. Winter, *J. Vac. Sci. Technol. A*, 2020, **38**, 12402.

48 W. A. Herrman, H. Ding, F. E. Kühn and W. Scherer, *Organometallics*, 1998, **17**, 2751-2757.

49 W. A. Herrman, G. Weichselbaumer, R. A. Paciello, R. A. Fischer, E. Herdtweck, J. Okuda and D. W. Marz, *Organometallics*, 1990, **9**, 489-496.

50 M. R. Cook, W. A. Herrman, P. Kiprof and J. Takacs, *J. Chem. Soc., Dalton Trans.*, 1991, 797-804.

51 W. A. Nugent, *Inorg. Chem.*, 1983, **22**, 965-969.

52 T. Schoop, H. W. Roesky, M. Noltemeyer and H.-G. Schmidt, *Organometallics*, 1993, **12**, 571-574.

53 W. A. Herrman, J. G. Kuchler, G. Weichselbaumer and E. Herdtweck and P. Kiprof, *J. Organomet. Chem.*, 1989, **372**, 351-370.

54 W. A. Herrman, G. Weichselbaumer and E. Herdtweck, *J. Organomet. Chem.*, 1989, **372**, 371-389.